Catalysis Letters (2019) 149:2415–2424
https://doi.org/10.1007/s10562-019-02848-x

Synthesis and Catalytic Applicability of Pt–Pd ITO Grown Nano Catalyst: An Excellent Candidate for Reduction of Toxic Hexavalent Chromium

Ali Muhammad Mahar[1] · Aamna Balouch[1] · Farah Naz Talpur[1] · Abdullah[1] · Sirajuddin[2] · Ameet Kumar[1] · Pirah Panah[1] · Muhammad Tariq Shah[1]

Received: 1 April 2019 / Accepted: 26 May 2019 / Published online: 12 June 2019

Abstract

In this study, we report the synthesis of indium tin oxide (ITO) decorated Pt–Pd nanoparticle by a simple and facile liquid phase deposition protocol and their application as a heterogeneous catalyst for the reduction of toxic hexavalent chromium. Different characterization techniques were used to confirm the synthesized nanoparticles are honeycomb-like structure. The average size of nanoparticles was found to be 2–5 nm and uniformly distributed over ITO surface. During this study, the parameter was optimized such as the effect of different reducing agent and their concentration, effect of microwaves radiation and dose of nanoparticles. It was observed that the kinetic mechanism was best describes by the pseudo-first order. The synthesized Pt–Pd nanoparticles were successfully applied as an excellent heterogeneous catalyst for reduction of Cr(VI) to Cr(III) in water. The synthesized nanocatalyst was good in term of fast kinetic, high catalytic efficiency, excellent recyclability, and analytical applicability for fast and efficient reduction of toxic hexavalent chromium as compared to conventional methods of nanocatalysts.

Graphic Abstract

Schematic illustration of hexavalent chromium reduction

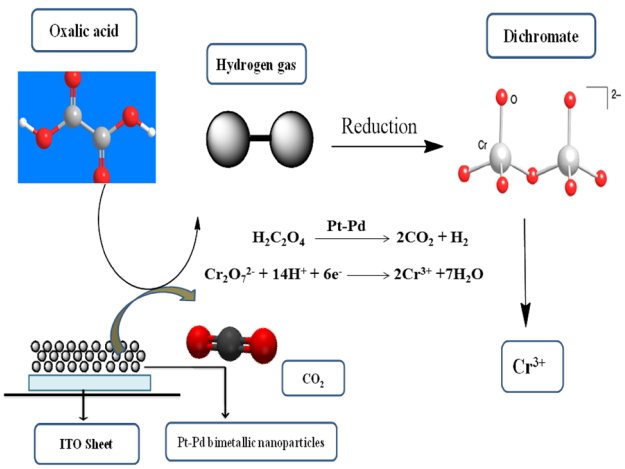

Keywords Pt–Pd bimetallic nanoparticles · Indium tin oxide (ITO) · Heterogeneous catalyst · Chromium

✉ Aamna Balouch
aamna_balouch@yahoo.com

Extended author information available on the last page of the article

1 Introduction

The hexavalent chromium compounds are considered as the most common pollutants which can play a vital role in causing acute toxicity, mutagenicity, and carcinogenicity [1, 2]. The wastewater of industrial processes such as leather tanning, lacquer production, electroplating and production of chromate contain Cr(VI) as a common contaminant. The toxicity and mobility of trivalent chromium are less as compared to hexavalent chromium [3–6]. The small amounts of Cr(III) are required for humans and animals as an important nutrient for the metabolism of sugars and fats [7]. Therefore, to avoid the environmental risks associated with Cr(VI) production sites, the development of advanced technologies is the highest need which can convert Cr(VI) to Cr(III) which is hazardous for living beings. For this purpose, nowadays different cheaper and practical techniques have been developed [7–15]. In these techniques, nanocatalysts of noble metals and their architectures have received much attention due to their porous surface, multiple-edged, fine tips, and fringes. These structures have profound activity in catalytic reactions due to greater interactions with reactants [16–29]. It has been studied that Pd nanoparticles with various morphologies and shapes used in a different type of redox reactions as catalysts [30–37]. Tilly and coworkers reported the synthesis and activity of branched like Pd nanocatalyst and confirmed the tetrapods of Pd nanoparticles in toluene solution [35]. In some other studies, the supported and solution phase nano tetrapods of Pd were synthesized in the solution of sodium dodecyl sulfate and N,N-dimethylformamide and these tetrapods proved as efficient catalysts [33, 34]. Sadik and colleagues synthesized the colloidal nanoparticles of Pd catalyst for the effective conversion of Cr(VI) to Cr(III) in the presence of formic acid. Dadapat et al. synthesized reusable Pd nanocatalyst, a thick film of these nanoparticles fused with mesoporous γ-Al_2O_3 were formed by using formic acid as a reducing agent. These films have proved to be an effective reusable catalyst for the conversion of Cr(VI) to Cr(III) [38, 39]. Fu and coworkers synthesized the arginine assisted Pd tetrapods and they have checked the catalytic activity for the reduction of Cr(VI) to Cr(III) [40]. However, these tetrapods have proved to be an efficient catalyst in the reduction of toxic pollutants, because these particles agglomerate together there is a problem to remove and reuse. Furthermore, their application as large scale hindered at industry level [41].To enhance catalytic applicability of Pd, by combining with Pt would significantly increase catalytic activity because of superior catalytic activity of Pt [42]. Furthermore, Pt is reliable to use suitable substrate to grow noble catalyst to enhance its catalytic applicability such as Graphene oxide, graphene reduced substrate to immobilize the metal catalyst [43, 44].

Dong-Ning Li and coworkers prepared Pt@Pd core–shell nanoparticles on supporting material N-doped reduced graphene oxide (Pt@Pd NCs/N-rGO) which showed enhanced catalytic activity and the problem of the reusability also improved but the synthesis of nanocrystals on reduced graphene oxide approach has complicated experimental procedure that reports high cost and time consuming [29, 45]. In our reported method, we have grown Pd nanocatalysts on ITO substrate and successfully applied as a heterogeneous catalyst [46].

In this study, we report a simple and facile liquid phase deposition route for Pt–Pd bimetallic nanocatalyst grown on ITO surface and their application as a heterogeneous catalyst for reduction of toxic hexavalent chromium to trivalent chromium. The synthesized nanocatalyst have high catalytic performance due to their highly porous honeycomb-like structure. Furthermore, they have fast kinetic, excellent reusability and good candidates for efficient reduction of toxic hexavalent chromium to trivalent chromium (99.8%) reduction using 50 µg catalyst within only a 100 s reaction time.

2 Experimental Work

2.1 Chemicals and Materials

All Chemicals used in the experiment were analytical grade and purchased from well-known suppliers and used as received without any further purification. Indium tin oxide substrate (ITO) was purchased from Vinkarola instrument, USA and metal precursors salts including Potassium hexachloroplatinate (K_2PtCl (IV)), Potassium hexachloropalladate (K_2PdCl (IV) and Potassium dichromate ($K_2Cr_2O_7$) were obtained from Fluka company. Also, Sodium Dodecyl Sulphate (SDS) and Polyvinyl Pyrrolidone (PVP) purchased from Fluka. Formic acid, Oxalic acid, Sodium borohydride, acetone, and ethanol were obtained from Sigma-Aldrich. Milli-Q water was used throughout experimental work.

2.2 Glassware's

All the glassware used in experimental work was washed using detergent and sonicated in the presence of 2% HNO_3 for 15 min after sonication rinsed thoroughly with Milli-Q water and finally dried in the oven.

2.3 Synthesis of Pt–Pd Bimetallic Nanocatalyst

Platinum-palladium bimetallic nanocatalyst was successfully synthesized on the surface of Indium tin oxide (ITO) glass slide (solid substrate) by simple and facile one-pot liquid phase deposition protocol in which the nanoparticles were directly grown on the surface of the solid substrate. The growth solution used in this method was the mixture of aqueous solutions of 1.0 mM K_2PtCl_6, 0.5 mM K_2PdCl_6, 10 mM sodium dodecyl sulfate, 0.5 $mmol^{-1}$ polyvinyl pyrrolidones, and 1.0 $mmol^{-1}$ formic acid. Initially, by the addition of metal precursor, the solution became dark brown but later turned yellow by the addition of reducing agent. After that, ITO slide (size 1×1.5 cm) was immersed up to 1.2 cm height and the reaction was proceeded at 45 °C with 400 rpm stirring. The color of the solution gradually changes from yellow to transparent and completely black color particles appeared on ITO slide in 40 min of reaction time. A black layer on the surface of the ITO substrate confirms the successful growth of Pt–Pd nanostructures. Surprisingly, the growth of nanoparticles was found only on the surface of ITO and not on the walls of the reaction vessel. Thus, this phenomenon shows the unique property of the liquid phase deposition (LPD) method we applied for the synthesis of Pt–Pd bimetallic NPs.

3 Results and Discussion

3.1 Characterization

3.1.1 TEM Analysis

The morphology of the hetero-aggregated Pt–Pd bimetallic NPs was characterized by transmission electron microscopy (TEM) at low and high resolutions as shown in Fig. 1a–d. The images at low magnification show that nanoparticles are arranged in a honeycomb-like structure shown in Fig. 1a, b, while the high magnification images show that honeycomb-like structure is composed of ultra-small nanoneedles like shape as shown in Fig. 1c, d. Further, it confirms the size of NPs ranges from 3 to 5 nm with an average size of 4 nm.

3.1.2 XRD Analysis

The crystalline structure and phase of synthesized bimetallic nanoparticles were examined by X-ray diffractometer as shown in Fig. 2. Three peaks at $2\theta = 40.20°$, 55.3°, and 77.6° were observed in the XRD spectra which are associated with Pt–Pd bimetallic system. Some additional peaks associated with ITO substrate could also be seen in Fig. 2. The XRD results were found in good agreement with the Joint committee of powder diffraction standards (JCPDS) card No. 05-0681. These results demonstrate the effectiveness of the

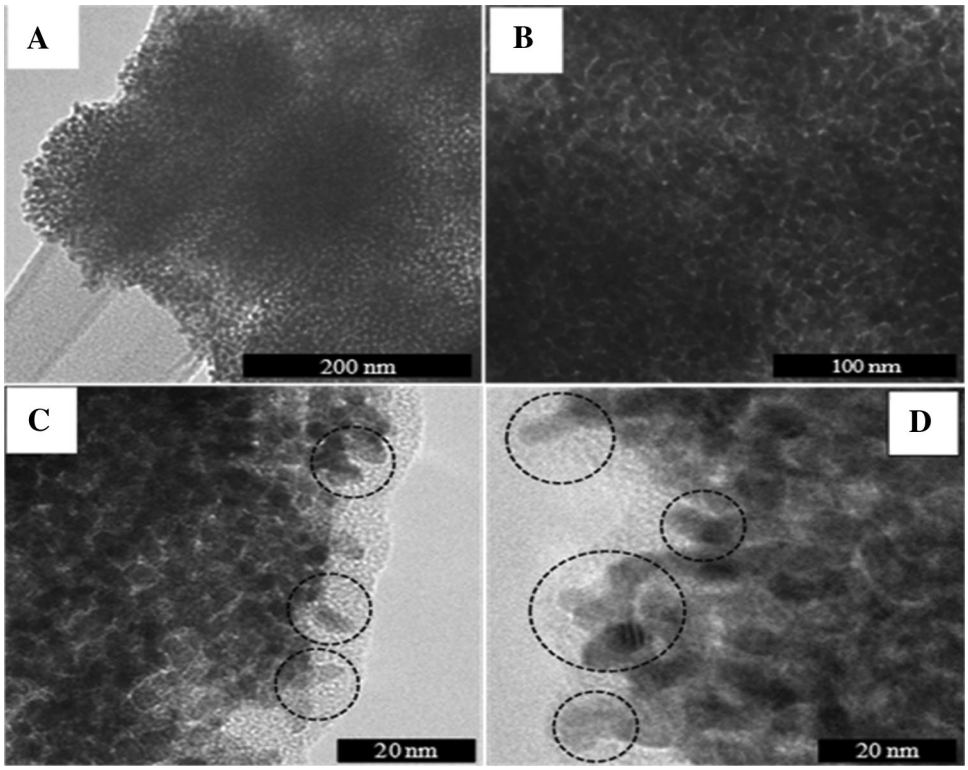

Fig. 1 TEM images of Pt–Pd@ ITO substrate. **a** and **b** at low resolution, **c** and **d** at high resolution

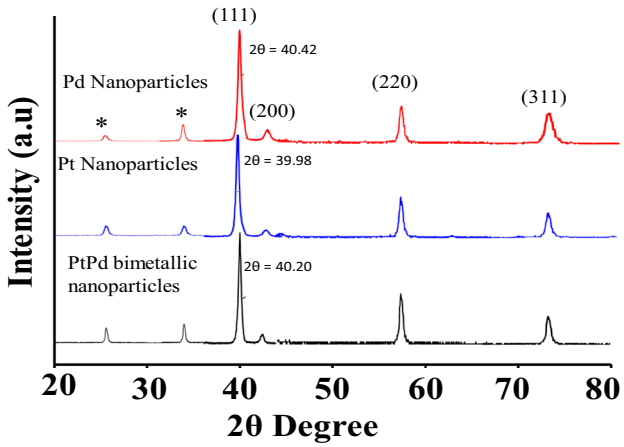

Fig. 2 XRD analysis of the Pt–Pd bimetallic nanoparticles on ITO substrate (Red line) Pd, (Blue line) Pt nanoparticles and (Black line) Pt–Pd bimetallic nanoparticles

approach for growing Pt–Pd BMNPs from the solution phase onto the surface of the substrate directly. When the Bragg's planes of bimetallic Pt–Pd nanoparticles at (111), (200) and (220) were compared with the pure Pt and Pd diffraction planes at these positions, a close resemblance was found in the diffraction planes with a little bit shifting as shown in Fig. 2. This little shift in the position of the plane could be due to the introduction of Pd metal into the host lattice of Pt. The position of Pt–Pd bimetallic nanostructure's peaks were compared with the lattice plane of pure Pt and Pd, and it is observed that the main peak of Pt–Pd is shifted about 0.22° from the peak of individual Pt and shifted about 0.22° from the peak of individual Pd as shown Fig. 2.

3.1.3 XPS Analysis

The X-ray photoelectron analysis was carried out to assess the chemical composition and binding energies of the synthesized Pt–Pd nanocomposites. Gaussian–Lorentzian (G–L) curve fitting process was used for the peak line shape and its background was Shirley-type. The components of Gaussian and Lorentzian were 70% and 30% respectively. The C^1s used as a calibration curve with a binding energy of 285 eV for the core level spectra. Figure 3a–c illustrate the characteristic low and high-resolution core level spectra of Pt (4f) and Pd (3d). Figure 3b demonstrates the appearance of Pt $4f^{7/2}$ curve with three spin–orbit pairs accompanied with its two oxidation states, such as Pt^0 at 71.37 eV (curve 1) and two peaks (curve 2 and curve 3) of Pt^{2+} with binding energies of 71.90 eV and 72.99 eV, which depicts its chemical state composition. This phenomenon shows the

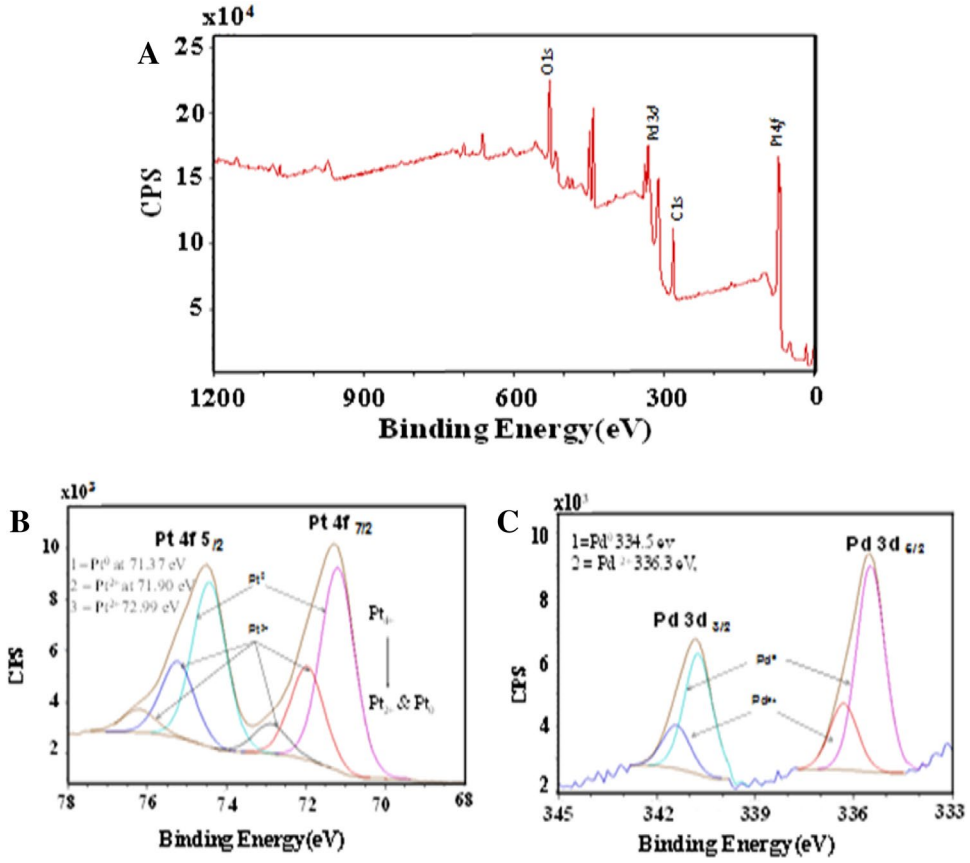

Fig. 3 XPS spectra of Pt–Pd bimetallic nanoparticles on ITO substrate **a** low magnification complete spectra, **b** Pt binding energy spectra at high resolution and (C) Pd binding energy spectra at high resolution

reduction in Pt, from Pt^{4+} to Pt^{0}. Figure 3c further illustrates Pd $3d^{5/2}$ with two spin–orbit pairs appeared one at 334.5 eV and second at 336 eV. Thus, showing two oxidation states namely Pd^{0} and Pd^{+2}. Two binding energy shifts, showing effective electron transfer from Pd to Pt, are easily noticeable. A positive shift is with Pt (to high energy level) and negative shift (to lower energy level) with Pd. This should be valid with the property of Pd as an electron donor, while the Pt as electron acceptor because of its f-orbital half-filled for bimetal formation.

4 Application and Optimization

4.1 Effect of Various Reducing Agents

At first, the type of reducing agent was checked by adding formic acid, Ascorbic acid, Oxalic acid, and sodium borohydride as shown in Fig. 4. The percent reduction of Cr(VI) to Cr(III) was achieved 3.1, 5, 7.9 and 18.3 for sodium borohydride, formic acid, ascorbic acid, and oxalic acid respectively. It was observed that organic acids are the more suitable reducing agent as compare to sodium borohydride. The best results were observed in oxalic acid it may because oxalic acid is one of the strongest organic acids and it is readily oxidized which makes it useful as a reducing agent for the reaction. Therefore, it was chosen for further study.

4.2 Effect of Oxalic Acid Concentration

The effect of oxalic acid concentration was initially monitored. In a typical procedure, different concentrations from 0.005 $mmol^{-1}$ to 0.025 $molL^{-1}$ oxalic acid were added in a reaction vessel containing 0.002 $molL^{-1}$ Cr(VI). The reaction was monitored for 4 min (240 s) results shown in Fig. 5. The spectrum demonstrates that increase in the

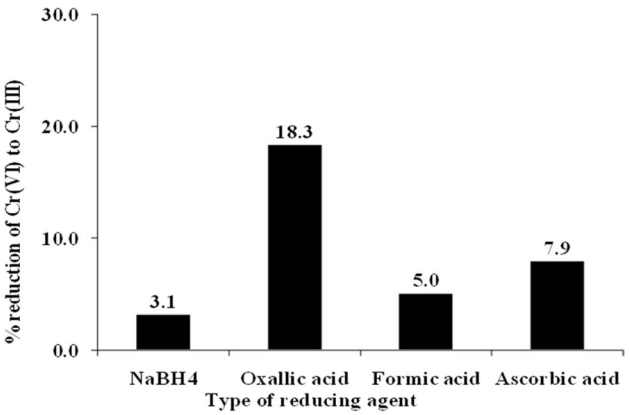

Fig. 4 Effect of different reducing agents for the reduction of Cr(VI) to Cr(III)

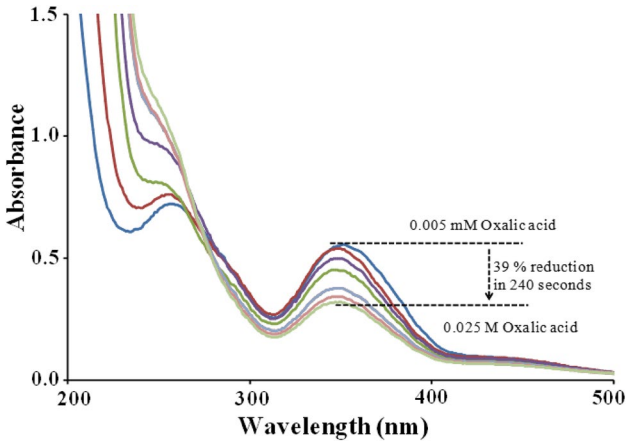

Fig. 5 Effect of oxalic acid concentration for the reduction of Cr(VI) to Cr(III)

concentration of oxalic acid from millimolar to molar without any initiator or catalyst did not show any spectral change of the Cr(VI) absorption band, hence no improvement was observed in reduction. Maximum 35% reduction was achieved with the use of 0.025 $molL^{-1}$ oxalic acids. Therefore, it was concluded that the amount of oxalic acid is not much effective without catalyst or initiator. Thereafter, the reaction was processed, and microwave radiations were introduced as the reaction initiator.

Generally, the hydrogenation process occurs when the oxalic acid reacts with the Pt–Pd bimetallic nanoparticles and forms carbon dioxide and hydrogen gas.

$$(HOOCCOOH \xrightarrow{Pt-Pd} 2CO_2 + H_2)$$

The result of decomposition of $C_2H_2O_4$ occurs at {111} fcc Pt–Pd bimetallic nanoparticles. Particularly, the adsorption of oxalic acid occurs at the surface of Pt–Pd bimetallic nanoparticles which decomposes the oxalic acid into CO_2 and H_2 which reduced the Cr(VI) into Cr(III) with the help of hydrogen transfer

$$(Cr_2O_7^{2-} + 14H^+ + 6e^- \rightarrow 2Cr^{3+} + 7H_2O)$$

4.3 Effect of Microwave Radiation Power

The microwave radiations were introduced as reaction initiator and MW power was optimized as shown in Fig. 6. In a typical procedure, the same amount of Cr(VI) was taken along with 0.001 M oxalic acid and the reaction was proceeded under microwave radiations. The reduction of Cr(VI) was measured by changing the power (0 to 1100 W). It was then observed that microwave can accelerate the reduction of Cr(VI) up to 50% at 110 W in 4 min (240 s). The further rise in the power of radiations from 110 W caused no significant increase in reduction. This could be due to the

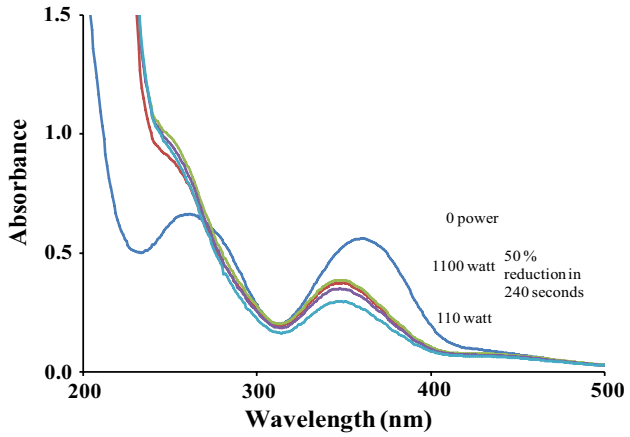

Fig. 6 UV–Visible spectrum of Cr(VI) reduction at different MW radiation power

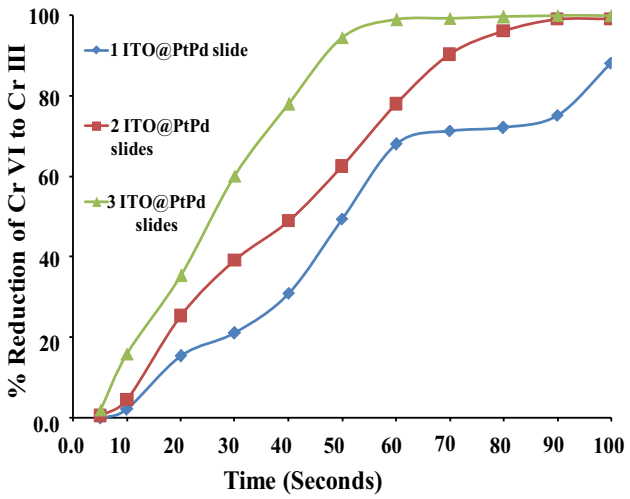

Fig. 7 Effect of catalyst dose on the reduction of Cr(VI) to Cr(III)

rise in temperature of reaction with an increase in power of microwave radiations which in turn does not favor the reaction in the forward direction. So, it is suggested that without catalyst only 50% Cr(VI) to Cr(III) transformation can be achieved.

4.4 Catalyst Dose Optimization

Finally, the effect of catalyst dose was also evaluated by increasing the number of Pt–Pd-decorated ITO slides as shown in Fig. 7. Initially, one ITO slide was added into the reaction vessel containing 0.002 M chromium, 0.005 mM under microwave radiations and the changes in Cr(VI) peak were monitored by the spectrophotometer. Figure 7 shows that one ITO slide which approximately containing 50 µg of Pt–Pd catalyst (Blue line) gradually decreased the concentration of chromium (VI) and maximum 88% reduction was achieved at 100 s of reaction time. As we increased the number of ITO slides (red line), 95% conversion is obtained within 80 s. Further, when we increased the amount of catalyst by putting 3 ITO slides (Green line), the results were much promising and 99.9% reduction of Cr(VI) was achieved within 100 s of reaction time. Hence, it was observed from these results that by increasing the amount of catalyst, the efficiency of Cr(VI) reduction was enhanced and the time to complete the conversion of Cr(VI) to Cr(III) was also reduced (Fig. 7).

5 Kinetic Study

The change in reduction with time is very crucial, for this purpose Lagergreen pseudo first order and the pseudo-second-order was used to determine the reduction capacity with time. The Lagergren first-order kinetic model equation can be written as follows:

$$\ln(q_e - q_t) = \ln q_e - \frac{k_1 t}{2.303}$$

The examination of Lagergren pseudo-first-order model was observed by plotting $\ln(q_e - q_t)$ against time (t) where q_e represents the quantity of chromium adsorbed on Pt–Pd@ITO(mg/g) at equilibrium, q_t is the quantity of chromium adsorbed on Pt–Pd@ITO at time t and k_1 is the rate constant of adsorption reaction. Linear correlation coefficient value of the first order is 0.99 as shown in Fig. 8a and from the slope of the plot also the values of rate constant K_1 and qe were evaluated as 0.476 min^{-1} and 2.505 mg g^{-1} respectively. The Lagergren second-order kinetic model equation can be written as follows:

$$\frac{t}{qt} = \frac{1}{k_2 qe^2} + \frac{1}{qe} t$$

where K_2 is the rate constant of pseudo-second order, in second order plot of $\frac{t}{qt}$ versus t is obtained in which correlation coefficient line is not linear having the value of 0.921 as shown in Fig. 8b and from the slop of plot the calculated values for K_2 and qe are 1246 mg^{-1} min^{-1} and 8×10^{-6}mg g^{-1} respectively. So, from the line of correlation coefficient it, is assessed that adsorption of Cr(VI) on Pt–Pd@ITO follows Lagergreen pseudo first order reaction. All obtained values for pseudo-first and second order are summarized in Table 1.

6 Reusability of Catalyst

To check the multiple time utilization of Pt–Pd bimetallic nanoparticles, reusability studies were carried out. The synthesized Pt–Pd bimetallic nanoparticles with good mechanical durability are essential to be recycled multiple times.

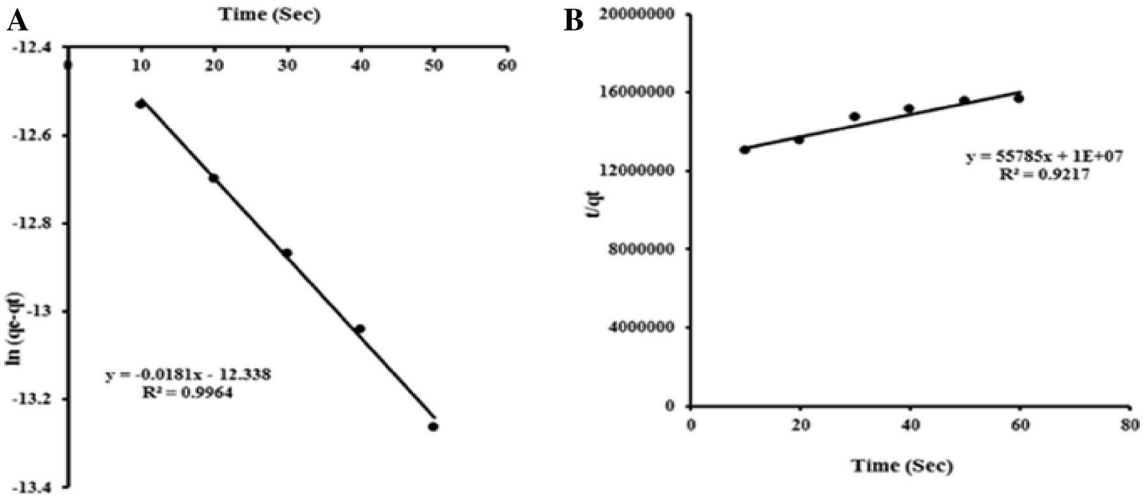

Fig. 8 **a** Lagergreen Pseudo-first and **b** Lagergreen pseudosecond-order kinetic model

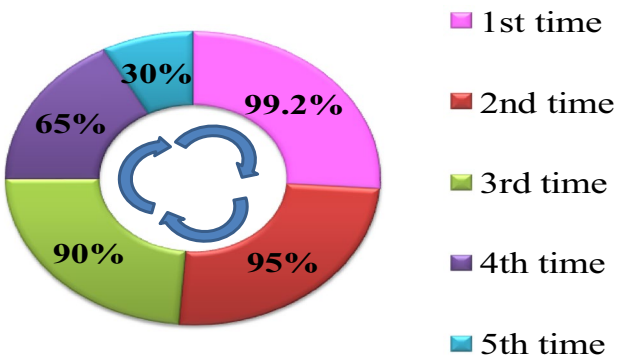

Fig. 9 Reusability study of nanocatalyst

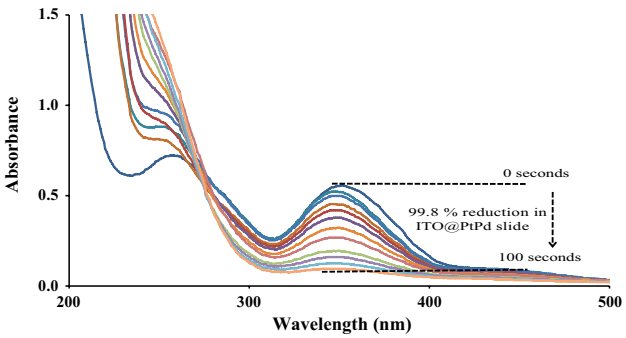

Fig. 10 UV–Visible spectra of Cr(VI) treated with Pt–Pd BMNPs@ITO in the presence of oxalic acid and MW radiations

Reduction of Cr(VI) ions was taken as a model reaction to check the efficiency with respect to the time. The catalytic performance of the Pt–Pd on ITO was studied for 5 different cycles. Before using in every next cycle ITO was washed by using deionized water and dried under nitrogen gas. It can be seen in the first cycle, 99.2% Cr(VI) was reduced and it was 95, 90, 65 and 30% for 2nd, 3rd, 4th, and 5th cycles respectively as shown in Fig. 9. Single ITO sheet (dimension 1.5×1.2 cm^2) contains 50 µg/mL Pt–Pd bimetallic nanocatalyst.

7 Comparison of Pt–Pd Nanocatalyst with Previously Reported Studies

Finally, we have also compared our work with the literature data, the bimetallic nanoparticles of Pt–Pd @ITO in the presence of oxalic acid have superior catalytic efficiency for the reduction of Cr(VI) among all the previous synthesized nanomaterials shown in Table 2 whether they are Bimetallic or monometallic nanoparticles. While taking one glance on Table 2 we can see Pd tetrapods, Pd–Cu HPANSs and Pd@GACs showing the rate constant values of 0.571, 0.447 and 0.4210 min^{-1} respectively and these values are superior to all other catalysts such Pt/Pd @Pro-ESM, Ag–Au/RGO and Pd@SiO_2–NH_2 summarized in the table. When Pt–Pd@ITO employed it shows the rate constant of 0.476 min^{-1}, which is superior to other reported data.

Table 1 Kinetic parameters for reduction of Cr(VI) to Cr(III)

Pseudo first order			Pseudo-second order		
K_1 (min^{-1})	Qe (mg g^{-1})	R^2	K_2 (mg^{-1} min^1)	Qe (mg g^{-1})	R^2
0.476	2.508	0.996	1246	8×10^{-6}	0.921

Table 2 Comparison of catalytic activity of Pt–Pd@ITO over other reported catalysts

Catalyst	Dose (g)	Size (nm)	Time (min)	Rate constant ($k\ min^{-1}$)	Ref.
Pd tetrapods	2.0	10 ± 2	5.0	0.571	[40]
Pt/Pd@Pro-ESM	1.5×10^{-2}	1.8–4.2	15	0.282	[7]
Pd@SiO_2–NH_2	1×10^{-2}	3.7	5.5	0.094	[47]
Ag–Au/RGO	5×10^{-4}	1–10	3.5	0.0004	[48]
Pd–Fe/NMC	8×10^{-3}	20–30	30	0.163	[49]
Pd–Cu HPANSs	2.0	3.7	8.0	0.447	[50]
Pd@GACs	2×10^{-3}	21 ± 0.3	15	0.4210	[51]
Pt–Pd@ITO	1.5×10^{-4}	3–5	1.4	0.476	Present work

8 Analytical Applicability of Pt–Pd Nanocatalyst

The catalytic applicability of Pt–Pd@ITO nano catalyst was checked for the reduction of Cr(VI) in aqueous solution under optimized conditions. In a typical process, Pt–Pd@ITO nano catalyst was added in 10 mL aqueous solution having 4.0 mL of 0.002 $molL^{-1}$ Potassium dichromate ($K_2Cr_2O_7$) and oxalic acid ($C_2H_2O_4$) of 0.001 $molL^{-1}$ and irradiated with 110-W microwave radiations. After every 5.0 s, 0.5 mL of radiated solution was withdrawn and diluted up to 2.0 mL and the reduction of Cr(VI) was monitored by UV–Visible spectrophotometer. The redox reaction of oxalic acid occurred when chromate and oxalic acid adsorbed on the surface of Pt–Pd NPs and as a result, hydrogen and carbon dioxide gases are liberated which reduce the Cr(VI) to Cr(III). Initially, the effect of Pt–Pd nanocatalyst supported on solid substrate ITO was observed when the color of analyte (Chromium VI) solution changed from yellow to colorless within 100 s indicated the reduction of Cr(VI) to the Cr(III) (yellow to colorless). About 99% reduction of Cr(VI) to Cr(III) was obtained within 100 s of radiation time. The formation of Cr(III) was confirmed by the addition of sodium hydroxide solution to the reduced solution of Cr(VI). The chromium solution turned green which is the indication of hexahydroxochromate (III) ions in the solution. It was observed that the catalytic reduction of Cr(VI) proceeds fast due to the presence of Pt–Pd bimetallic nanoparticles as shown in Fig. 10.

9 Conclusion

In summary, the successful synthesis of Pt–Pd nanocatalysts decorated on the ITO surface by one-pot liquid phase deposition protocol. The synthesized nanocatalysts are highly porous and distributed throughout the ITO surface and arranged in a honeycomb-like structure. Various parameters were optimized during this study to enhance the catalytic efficiency of synthesized nanocatalyst such as concentration and type of reducing agent, dose, microwave radiation power, and reaction time. The synthesized nanocatalyst was successfully applied for catalytic reduction of toxic hexavalent chromium to trivalent chromium, with the 99.8% efficiency using 50 µg catalyst within only a 100-s reaction time. The synthesized nanocatalyst was good in term of fast kinetic, high catalytic efficiency, excellent recyclability, and analytical applicability for fast and efficient reduction of toxic hexavalent chromium.

References

1. Huang Y, Ma H, Wang S, Shen M, Guo R, Cao X, Zhu M, Shi X (2012) Efficient catalytic reduction of hexavalent chromium using palladium nanoparticle-immobilized electrospun polymer nanofibers. ACS Appl Mater Interfaces 4:3054–3061
2. Kumar A, Balouch A, Pathan AA, Abdullah, Jagirani MS, Mahar AM, Rajput M-U-H (2019) Novel chromium imprinted polymer: synthesis, characterization and analytical applicability for the selective remediation of Cr(VI) from an aqueous system. Int J Environ Anal Chem. https://doi.org/10.1080/03067319.2019.1599876
3. Bhowmik K, Mukherjee A, Mishra MK, De G (2014) Stable Ni nanoparticle–reduced graphene oxide composites for the reduction of highly toxic aqueous Cr(VI) at room temperature. Langmuir 30:3209–3216
4. Krishnani KK, Srinives S, Mohapatra B, Boddu VM, Hao J, Meng X, Mulchandani A (2013) Hexavalent chromium removal mechanism using conducting polymers. J Hazard Mater 252:99–106
5. Wu J-H, Shao F-Q, Han S-Y, Bai S, Feng J-J, Li Z, Wang A-J (2019) Shape-controlled synthesis of well-dispersed platinum nanocubes supported on graphitic carbon nitride as advanced visible-light-driven catalyst for efficient photoreduction of hexavalent chromium. J Colloid Interface Sci 535:41–49
6. Kumar A, Balouch A, Pathan AA, Mahar AM, Abdullah MS, Jagirani FA, Mustafai M, Zubair B Laghari, Panah P (2017) Remediation techniques applied for aqueous system contaminated by toxic Chromium and Nickel ion. Geol Ecol Landsc 1:143–153
7. Wei L-L, Gu R, Lee J-M (2015) Highly efficient reduction of hexavalent chromium on amino-functionalized palladium nanowires. Appl Catal B 176:325–330
8. Omole MA, Okello VA, Lee V, Zhou L, Sadik OA, Umbach C, Sammakia B (2011) Catalytic reduction of hexavalent chromium using flexible nanostructured poly (amic acids). ACS Catal 1:139–146

9. Park D, Yun Y-S, Park JM (2004) Reduction of hexavalent chromium with the brown seaweed Ecklonia biomass. Environ Sci Technol 38:4860–4864
10. Patterson RR, Fendorf S, Fendorf M (1997) Reduction of hexavalent chromium by amorphous iron sulfide. Environ Sci Technol 31:2039–2044
11. Wu J-H, Shao F-Q, Luo X-Q, Xu H-J, Wang A-J (2019) Pd nanocones supported on g-C3N4: an efficient photocatalyst for boosting catalytic reduction of hexavalent chromium under visible-light irradiation. Appl Surf Sci 471:935–942
12. Hu L-Y, Chen L-X, Liu M-T, Wang A-J, Wu L-J, Feng J-J (2017) Theophylline-assisted, eco-friendly synthesis of PtAu nanospheres at reduced graphene oxide with enhanced catalytic activity towards Cr(VI) reduction. J Colloid Interface Sci 493:94–102
13. Ye S, Zeng G, Wu H, Zhang C, Dai J, Liang J, Yu J, Ren X, Yi H, Cheng M (2017) Biological technologies for the remediation of co-contaminated soil. Crit Rev Biotechnol 37:1062–1076
14. Ye S, Zeng G, Wu H, Zhang C, Liang J, Dai J, Liu Z, Xiong W, Wan J, Xu P (2017) Co-occurrence and interactions of pollutants, and their impacts on soil remediation—a review. Crit Rev Environ Sci Technol 47:1528–1553
15. Ye S, Zeng G, Wu H, Liang J, Zhang C, Dai J, Xiong W, Song B, Wu S, Yu J (2019) The effects of activated biochar addition on remediation efficiency of co-composting with contaminated wetland soil. Resour Conserv Recycl 140:278–285
16. Yang S, Luo X (2014) Mesoporous nano/micro noble metal particles: synthesis and applications. Nanoscale 6:4438–4457
17. Zhang H, Jin M, Xia Y (2012) Noble-metal nanocrystals with concave surfaces: synthesis and applications. Angew Chem Int Ed 51:7656–7673
18. Quan Z, Wang Y, Fang J (2012) High-index faceted noble metal nanocrystals. Acc Chem Res 46:191–202
19. Cheong S, Watt JD, Tilley RD (2010) Shape control of platinum and palladium nanoparticles for catalysis. Nanoscale 2:2045–2053
20. Xiong Y, Xia Y (2007) Shape-controlled synthesis of metal nanostructures: the case of palladium. Adv Mater 19:3385–3391
21. Chen J, Lim B, Lee EP, Xia Y (2009) Shape-controlled synthesis of platinum nanocrystals for catalytic and electrocatalytic applications. Nano Today 4:81–95
22. Gong M, Fu G, Chen Y, Tang Y, Lu T (2014) Autocatalysis and selective oxidative etching induced synthesis of platinum–copper bimetallic alloy nanodendrites electrocatalysts. ACS Appl Mater Interfaces 6:7301–7308
23. Cunci L, Velez CA, Perez I, Suleiman A, Larios E, José-Yacamán M, Watkins JJ, Cabrera CR (2014) Platinum electrodeposition at unsupported electrochemically reduced nanographene oxide for enhanced ammonia oxidation. ACS Appl Mater Interfaces 6:2137–2145
24. Nguyen T-T, Pan C-J, Liu J-Y, Chou H-L, Rick J, Su W-N, Hwang B-J (2014) Functional palladium tetrapod core of heterogeneous palladium–platinum nanodendrites for enhanced oxygen reduction reaction. J Power Sources 251:393–401
25. Wang Q, Wang Y, Guo P, Li Q, Ding R, Wang B, Li H, Liu J, Zhao X (2014) Formic acid-assisted synthesis of palladium nanocrystals and their electrocatalytic properties. Langmuir 30:440–446
26. Chen M, Wu B, Yang J, Zheng N (2012) Small adsorbate-assisted shape control of Pd and Pt nanocrystals. Adv Mater 24:862–879
27. Hu B, Ding K, Wu T, Zhou X, Fan H, Jiang T, Wang Q, Han B (2010) Shape controlled synthesis of palladium nanocrystals by combination of oleylamine and alkylammonium alkylcarbamate and their catalytic activity. Chem Commun 46:8552–8554
28. Wang Y, Xie S, Liu J, Park J, Huang CZ, Xia Y (2013) Shape-controlled synthesis of palladium nanocrystals: a mechanistic understanding of the evolution from octahedrons to tetrahedrons. Nano Lett 13:2276–2281
29. Li D-N, Shao F-Q, Feng J-J, Wei J, Zhang Q-L, Wang A-J (2018) Uniform Pt@ Pd nanocrystals supported on N-doped reduced graphene oxide as catalysts for effective reduction of highly toxic chromium (VI). Mater Chem Phys 205:64–71
30. Zhao R, Fu G, Zhou T, Chen Y, Zhu X, Tang Y, Lu T (2014) Multi-generation overgrowth induced synthesis of three-dimensional highly branched palladium tetrapods and their electrocatalytic activity for formic acid oxidation. Nanoscale 6:2776–2781
31. Chu Y-T, Chanda K, Lin P-H, Huang MH (2012) Aqueous phase synthesis of palladium tripod nanostructures for Sonogashira coupling reactions. Langmuir 28:11258–11264
32. Zhu H, Li G, Chi Q, Zhao Y, Liu H, Li J, Huang T (2012) Controlled synthesis of tetrapod/Mitsubishi-like palladium nanocrystals. CrystEngComm 14:1531–1533
33. Dai Y, Mu X, Tan Y, Lin K, Yang Z, Zheng N, Fu G (2012) Carbon monoxide-assisted synthesis of single-crystalline Pd tetrapod nanocrystals through hydride formation. J Am Chem Soc 134:7073–7080
34. Zhu H, Li G, Lv X, Zhao Y, Huang T, Liu H, Li J (2014) Controlled synthesis of hierarchical tetrapod Pd nanocrystals and their enhanced electrocatalytic properties. RSC Adv 4:6535–6539
35. Watt J, Young N, Haigh S, Kirkland A, Tilley RD (2009) Synthesis and structural characterization of branched palladium nanostructures. Adv Mater 21:2288–2293
36. Shao F-Q, Feng J-J, Lin X-X, Jiang L-Y, Wang A-J (2017) Simple fabrication of AuPd@ Pd core-shell nanocrystals for effective catalytic reduction of hexavalent chromium. Appl Catal B 208:128–134
37. Balouch A, Umar A (2016) Heterogeneous catalytic degradation of nitro-aromatic compound using highly defect spongy surface palladium nanocatalyst. Nucleus 53:64–69
38. Omole MA, K'Owino IO, Sadik OA (2007) Palladium nanoparticles for catalytic reduction of Cr(VI) using formic acid. Appl Catal B 76:158–167
39. Dandapat A, Jana D, De G (2011) Pd nanoparticles supported mesoporous γ-Al_2O_3 film as a reusable catalyst for reduction of toxic CrVI to CrIII in aqueous solution. Appl Catal A 396:34–39
40. Fu G-T, Jiang X, Wu R, Wei S-H, Sun D-M, Tang Y-W, Lu T-H, Chen Y (2014) Arginine-assisted synthesis and catalytic properties of single-crystalline palladium tetrapods. ACS Appl Mater Interfaces 6:22790–22795
41. Liang M, Su R, Qi W, Zhang Y, Huang R, Yu Y, Wang L, He Z (2014) Reduction of hexavalent chromium using recyclable Pt/Pd nanoparticles immobilized on procyanidin-grafted eggshell membrane. Ind Eng Chem Res 53:13635–13643
42. Hu H, Xin JH, Hu H, Wang X, Miao D, Liu Y (2015) Synthesis and stabilization of metal nanocatalysts for reduction reactions—a review. J Mater Chem A 3:11157–11182
43. Xie Y, Li H, Tang C, Li S, Li J, Lv Y, Wei X, Song Y (2014) A high-performance electrocatalyst for oxygen reduction based on reduced graphene oxide modified with oxide nanoparticles, nitrogen dopants, and possible metal-NC sites. J Mater Chem A 2:1631–1635
44. Ehsani A, Shiri HM, Kowsari E, Safari R, Shayeh JS, Barbary M (2017) Electrosynthesis, physioelectrochemical and theoretical investigation of poly ortho aminophenol/magnetic functional graphene oxide nanocomposites as novel and hybrid electrodes for highly capacitive pseudocapacitors. J Colloid Interface Sci 490:695–702
45. Ye S, Yan M, Tan X, Liang J, Zeng G, Wu H, Song B, Zhou C, Yang Y, Wang H (2019) Facile assembled biochar-based nanocomposite with improved graphitization for efficient photocatalytic activity driven by visible light. Appl Catal B. https://doi.org/10.1016/j.apcatb.2019.03.004
46. Balouch A, Ali Umar A, Shah AA, Mat Salleh M, Oyama M (2013) Efficient heterogeneous catalytic hydrogenation of acetone

to isopropanol on semihollow and porous palladium nanocatalyst. ACS Appl Mater Interfaces 5:9843–9849
47. Celebi M, Yurderi M, Bulut A, Kaya M, Zahmakiran M (2016) Palladium nanoparticles supported on amine-functionalized SiO_2 for the catalytic hexavalent chromium reduction. Appl Catal B 180:53–64
48. Vellaichamy B, Periakaruppan P (2016) A facile, one-pot and eco-friendly synthesis of gold/silver nanobimetallics smartened rGO for enhanced catalytic reduction of hexavalent chromium. RSC Adv 6:57380–57388
49. Li S, Tang L, Zeng G, Wang J, Deng Y, Wang J, Xie Z, Zhou Y (2016) Catalytic reduction of hexavalent chromium by a novel nitrogen-functionalized magnetic ordered mesoporous carbon doped with Pd nanoparticles. Environ Sci Pollut Res 23:22027–22036
50. Han S-H, Bai J, Liu H-M, Zeng J-H, Jiang J-X, Chen Y, Lee J-M (2016) One-pot fabrication of hollow and porous Pd–Cu alloy nanospheres and their remarkably improved catalytic performance for hexavalent chromium reduction. ACS Appl Mater Interfaces 8:30948–30955
51. Veerakumar P, Thanasekaran P, Lin K-C, Liu S-B (2017) Biomass derived sheet-like carbon/palladium nanocomposite: an excellent opportunity for reduction of toxic hexavalent chromium. ACS Sustain Chem Eng 5:5302–5312

Affiliations

Ali Muhammad Mahar[1] · Aamna Balouch[1] · Farah Naz Talpur[1] · Abdullah[1] · Sirajuddin[2] · Ameet Kumar[1] · Pirah Panah[1] · Muhammad Tariq Shah[1]

[1] National Centre of Excellence in Analytical Chemistry, University of Sindh, Jamshoro, Pakistan

[2] HEJ Research Institute of Chemistry, International Center for Chemical and Biological Sciences, University of Karachi, Karachi 75270, Pakistan